IEEE Photonics Journal
An IEEE Photonics Society Publication

Ultracompact TM-Pass Silicon Nanophotonic Waveguide Polarizer and Design

Volume 2, Number 1, February 2010

Qian Wang, Member, IEEE
Seng-Tiong Ho

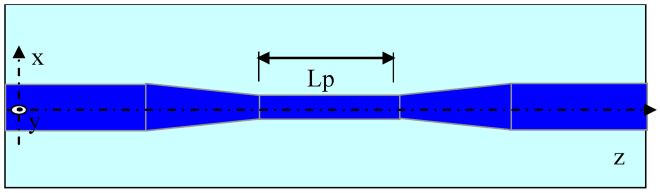

Silicon waveguide based TM-pass polarizer

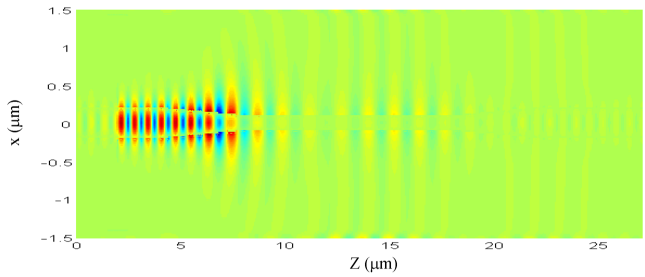

FDTD simulation of TE mode propagation

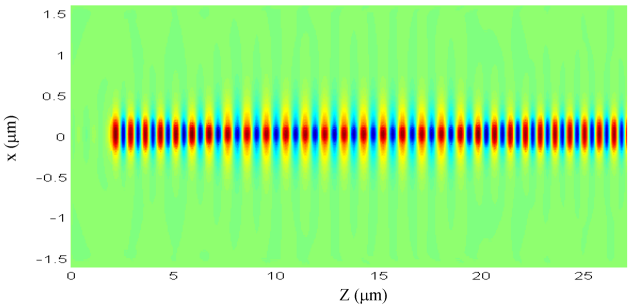

FDTD simulation of TM mode propagation

DOI: 10.1109/JPHOT.2010.2041650
1943-0655/$26.00 ©2010 IEEE

Ultracompact TM-Pass Silicon Nanophotonic Waveguide Polarizer and Design

Qian Wang,[1] ***Member, IEEE*, and Seng-Tiong Ho**[2]

[1]Agency for Science, Technology and Research, Data Storage Institute, Singapore 117608
[2]Department of Electrical Engineering and Computer Science, Northwestern University, Evanston, IL 60208 USA

DOI: 10.1109/JPHOT.2010.2041650

Manuscript received December 11, 2009; revised January 15, 2010. First published Online January 22, 2010. Current version published February 12, 2010. Corresponding author: Q. Wang (e-mail: qian.wang@osamember.org).

Abstract: An ultracompact transverse magnetic (TM)-pass polarizer based on silicon nanophotonic waveguides is proposed, which contains two tapered waveguides sandwiching a narrow waveguide section only supporting TM-mode propagation. A full-vectorial eigenmode solver is employed to determine the appropriate cross section of the silicon nanophotonic waveguide. The device is first designed in a 2-D approximate model using a wide-angle beam propagation method, and numerical verification is carried out afterward using a parallel full-vectorial 3-D finite-difference time-domain simulation. Both approaches indicate that the finite thickness of the buried SiO_2 layer and the reflection at the substrate play important roles on the extinction ratio of the device. A designed numerical example shows an extinction ratio of $\sim$26 dB for the waveguide polarizer with a length of $\sim$10 μm, while the insertion loss for the TM mode is negligible.

Index Terms: Silicon nanophotonics, waveguides.

1. Introduction

Silicon nanophotonic waveguide using silicon-on-insulator (SOI) substrate is emerging as a promising technique for high-density integration due to strong light confinement and compatibility with complementary metal-oxide-semiconductor (CMOS) technology [1]. Various ultrasmall devices based on silicon nanophotonic waveguides used for data transfer, information processing, and optical sensing have been demonstrated in recent published investigations, which include couplers, ring resonator filters, planar grating-based wavelength multiplexers, etc. [1]–[6]. For the optical sensing utilizing the evanescent field or surface plasmon mode on silicon photonic waveguide, the Transverse Magnetic (TM) mode is desired for its higher sensitivity, as compared with the Transverse Electric (TE) mode [7]. Hence, a novel and ultracompact polarizing structure based on nanophotonic waveguide is proposed and designed in this paper, which is also an essential element used in coherent optical information processing.

Various types of waveguide polarizers have been proposed and demonstrated recently using, for example, metal-cladding, birefrigent material, nanocomposite film, slot waveguides, etc. [8]–[13]. Some of these waveguide polarizers have specific requirement on materials or fabrications. In this paper, we propose a waveguide polarizer utilizing the polarization dependence of light propagation within silicon nanophotonic waveguide. The structure proposed is schematically presented in Fig. 1 (Fig. 1(a) is the top view; Fig. 1(b) and (c) are, respectively, the cross section in the x–y plane of the input (output)

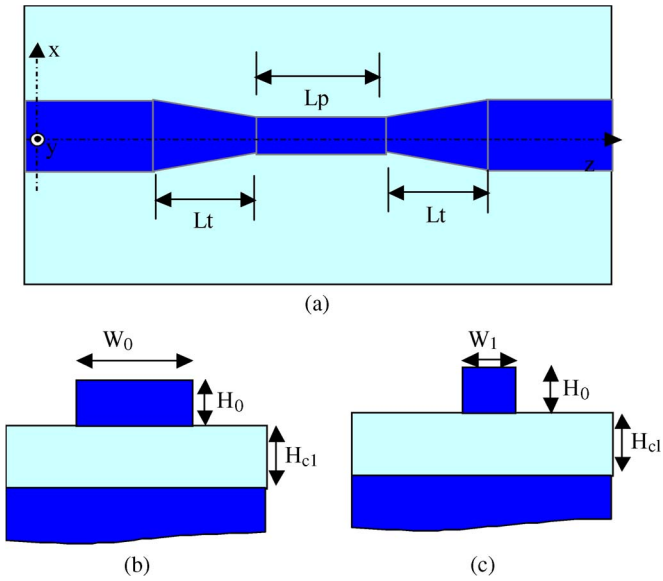

Fig. 1. TM-pass polarizer based on a tapering structure. (a) Top view; (b) cross section of the polarizer at the input and output position; (c) cross section of the polarizer at the central section.

waveguide and the central waveguide section). The waveguide polarizer contains two tapered waveguides sandwiching a central waveguide section, which is expected to support only TM-mode (the main electric component is E_y) propagation. For the TE mode (the main electric component is E_x), the central waveguide section is under the cutoff condition, i.e., light will radiate away while propagating along the device. Optical design of this silicon nanophotonic waveguide for a high extinction ratio with a ultracompact size consists of two steps: designing the silicon nanophotonic waveguide cross section for single-polarization propagation through eigenmode analysis and optimizing the device's extinction ratio through simulating light propagation in the whole device.

Section 2 presents a detailed analysis of the modal characterization of silicon nanophotonic waveguide using the full-vectorial eigenmode solution. Mode numbers and polarization dependence are investigated under different width and height of the core, which determines the cross section of the silicon waveguide for single-TM-polarization-mode propagation. Calculations show that for a silicon nanophotonic waveguide with a thickness of 300 nm, it only supports the TM-mode propagation when the width is less than 250 nm. The thickness of the buried SiO_2 layer is also analyzed due to the consideration of leakage loss to the substrate of the propagating TM light.

In Section 3, an approximate but fast design of the whole device is carried out using a 2-D model in the *y*–*z* plane after the effective index method in the *x*-direction. Simulation of light propagation in this approximate model using a wide-angle beam propagation method [14] shows that the finite thickness of the SiO_2 layer and the leaky light of the TE mode reflected back from the substrate play important roles on the extinction ratio of the device. Following this approximate design, a rigorous numerical verification of light propagation in the device is carried out using a parallel 3-D finite-difference time-domain (3-D FDTD) [15]. The numerical example shows that by using a total length of 18 μm (length for the central region is 10 μm and length for the two tapered sections is 8 μm), an extinction ratio of $\sim$26 dB can be achieved for the silicon nanophotonic waveguide when the thickness of the buried SiO_2 layer is 1.5 μm. The insertion loss of the TM mode for this nanophotonic waveguide polarizer designed is negligible. Conclusions are drawn in Section 4.

2. Silicon Nanophotonic Waveguide Supporting Single Polarization Mode

Fig. 1(b) presents a typical cross section of the silicon nanophotonic waveguide based on an SOI substrate. The width and height of silicon nanophotonic waveguide core is *W* and *H*. The buried

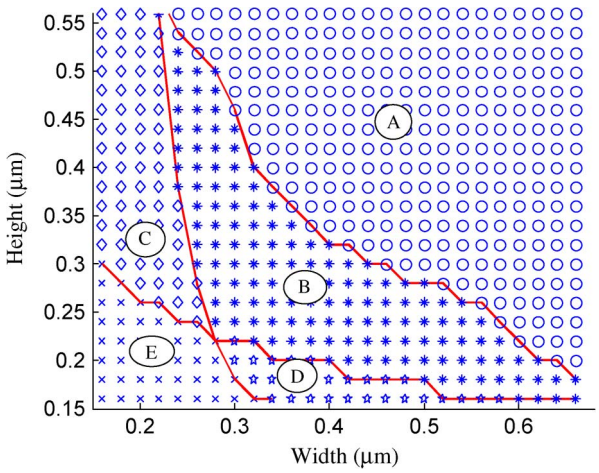

Fig. 2. Modal characteristics of silicon nanophotonic waveguide with different width and height.

silicon dioxide layer has a thickness of H_{cl}. The refractive index of the silicon is 3.477, and the buried silicon dioxide is 1.45 at wavelength 1550 nm. The top cladding is air. A full-vectorial eigenmode solution is employed with a modified finite-difference scheme, as proposed in [16] and [17] to investigate the modal characterization of silicon nanophotonic waveguide. Eigenmodes of silicon nanophotonic waveguide with a width W ranging from 0.16 μm to 0.66 μm and height H from 0.16 μm to 0.56 μm are calculated. Based on the comparison between the effective refractive index calculated and refractive index of SiO_2 cladding layer and TE percentage of the guided mode, the modal characteristics of the silicon nanophotonic waveguide are presented in Fig. 2, which consists of five regions labeled from A to E with different marks, namely Region A: multimode region; Region B: single-mode region; Region C: single-TM-mode region; Region D: single-TE-mode region; and Region E: cutoff region.

It can be seen that for this silicon nanophotonic waveguide besides the multimode region A and single-mode region B, there are two so-called single-polarization-mode regions which support only one polarization state. Waveguide with a cross section in Region C only supports TM mode, while for Region D, it only supports TE mode. The existence of single-polarization-mode region is due to the highly polarization dependence of silicon nanophotonic waveguide, which leads to the different cutoff conditions between the TE and TM modes.

For this silicon nanophotonic waveguide to act as a polarizer, we choose the thickness of waveguide core to be 300 nm. According to the modal characteristics presented in Fig. 2, the thinner silicon waveguide reduces the difference of the corresponding waveguide width of the cutoff condition between the TM and TE modes. A thicker waveguide requires a smaller width for single-mode condition, which is not recommended in practice while taking account of the etching surface roughness. Therefore, the 300-nm-thick waveguide is appropriate not only for this silicon nanophotonic waveguide polarizer but for integrating other photonic devices that require single-mode propagation as well. The effective refractive indices of the TE and TM modes the waveguide with a thickness of 300 nm under different waveguide widths are shown in Fig. 3, which shows that when the width of the waveguide is between 250 nm and $\sim$180 nm, the waveguide will only support the TM mode. Therefore, in our design example, we choose the width of the central waveguide section to be 200 nm.

The buried SiO_2 layer of the SOI wafer with a sufficient thickness is very important while taking account of the propagation loss of TM mode in the central region due to the leakage in the silicon substrate (in the next section, the thickness of the buried SiO_2 layer is shown to also have a significant influence on the extinction ratio of the device). Here, the eigenmode solution with a perfectly matching layer-boundary condition is used to calculate the leakage loss of the TM mode. The propagation loss coefficient α for characterization of the leakage loss is defined to be

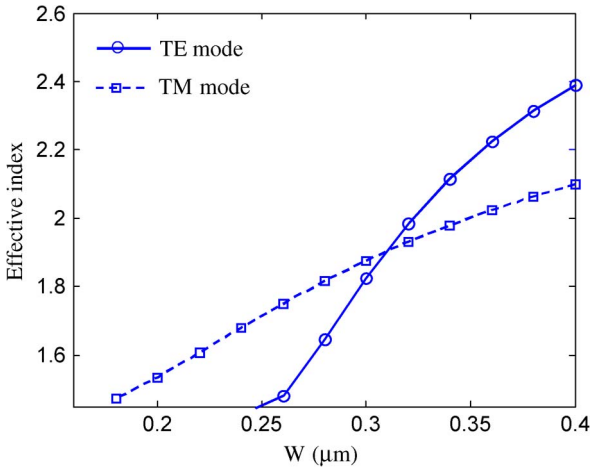

Fig. 3. Effective indices of the TE and TM modes under different widths of the silicon nanophotonic waveguide when H = 300 nm.

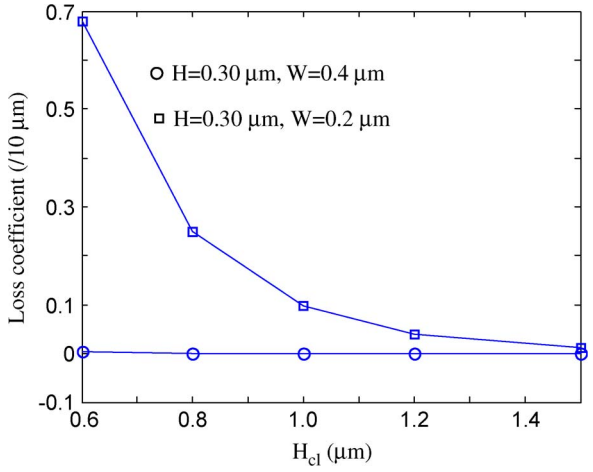

Fig. 4. Propagation loss coefficient of the TM mode under different buried cladding layer thickness.

$\alpha = (4\pi/\lambda)\mathrm{Im}(n_{eff})$, where $\mathrm{Im}(n_{eff})$ is the imaginary part of the effective refractive index. For the central waveguide section, the propagation loss coefficient is calculated (see Fig. 4). From this calculation result, it can be seen that when the thickness of buried SiO_2 is no less than 1 μm, the central TM-pass waveguide has a negligible propagation loss when the length of the central section is on a scale of tens of micrometers.

3. Optical Design of TM-Pass Polarizer Through Simulating Light Propagation

Two waveguides linearly tapered are used as the transition between the single-mode input/output waveguides and the central waveguide with the single polarization mode to minimize the insertion loss for the TM mode [see Fig. 1(a)]. The width of the single-mode input/output waveguide is chosen to be 400 nm. The length of the tapered waveguide is $L_t = 4$ μm, which is sufficient for adiabatic tapering from 400 nm to 200 nm, as shown the simulation below. To achieve a high extinction ratio with a compact size, the length of the central TM-pass waveguide section is optimized, and the influence of the thickness of buried oxide is analyzed in this section.

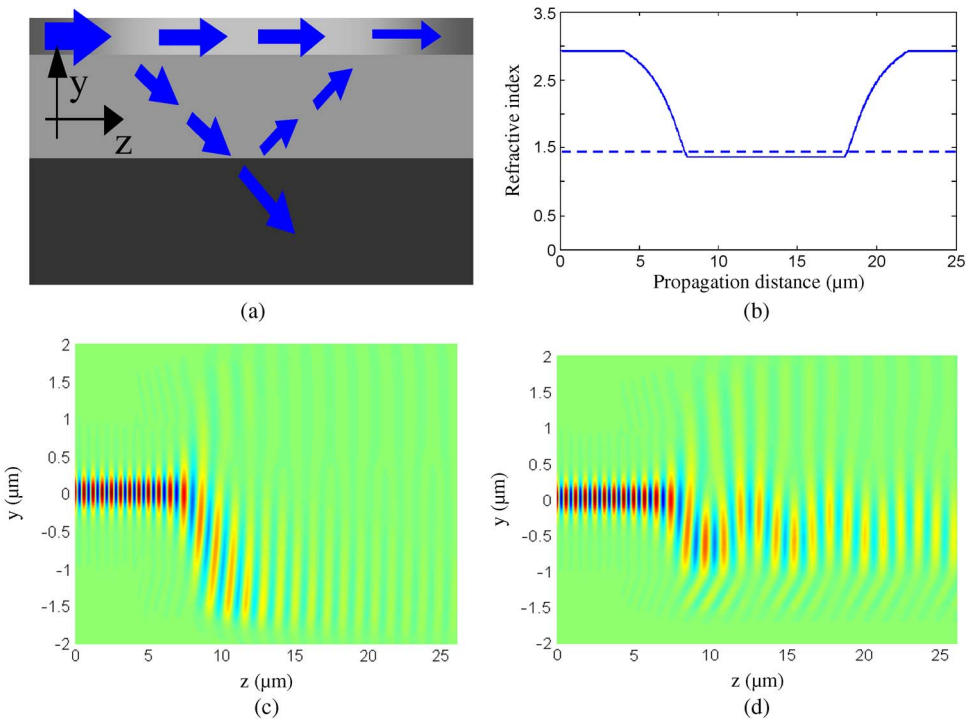

Fig. 5. (a) Approximate 2-D model of the waveguide polarizer after effective index method. (b) Effective index of the waveguide core in the 2-D model. (c) Light propagation in the case of semi-infinite cladding. (d) Light propagation in the case of finite thickness for the cladding layer.

To carry out a fast design, the waveguide polarizer is converted into an approximate 2-D model [see Fig. 5(a)] in the *y*–*z* plane by applying the effective index method in the *x*-direction. The waveguide in the 2-D model has a top cladding of air, a bottom-cladding layer of SiO_2, and silicon substrate. The refractive index of the core in the 2-D model is the effective index of the TM mode for an air-silicon-air planar waveguide in the *x*-direction. Therefore, the refractive index of the core in the 2-D model depends on the width of the silicon nanophotonic waveguide. As the width of silicon waveguide is decreased, the refractive index of the waveguide core in the 2-D model becomes smaller, and it is less than that of the buried SiO_2 in the central section, as shown in Fig. 5(b). For a waveguide with a semi-infinite bottom cladding, it is obvious that the longer TM-pass waveguide section corresponds to higher extinction ratio. However, in practice, the buried oxide layer has a finite thickness, and the radiated light of the TE mode penetrating through the buried cladding layer will be reflected at the interface between the cladding and substrate. Furthermore, the light reflected will couple with the propagating mode and affect the extinction ration significantly. Fig. 5(c) and (d) show the different propagating pattern of radiated light between the case of semi-infinite cladding and the buried SiO_2 layer with a thickness of 1 μm.

To evaluate the performance of the proposed waveguide polarizer, the radiation loss for the TE mode is calculated using a wide-angle beam-propagation method and overlap integral under a different length of the central waveguide, as well as the thickness of the buried SiO_2 layer. In this numerical example, four cases are chosen, i.e., $H_{cl} = 1$ μm, 1.5 μm, 2 μm, and semi-infinite. The corresponding insertion losses for the TE mode are presented in Fig. 6. It can be seen that with a semi-infinite buried silicon dioxide cladding layer, the insertion loss for the TE mode increases with length of central waveguide. However, for the other three cases, it is shown that finite thickness of the buried silicon dioxide layer has two significant influences on the insertion loss: 1) The insertion loss degrades due the existence of the substrate because the radiated light is quasi-confined and propagates in the buried dioxide layer, as seen in Fig. 5(d); 2) the insertion loss does not increase monotonously with the length of central waveguide section because of the coupling between the

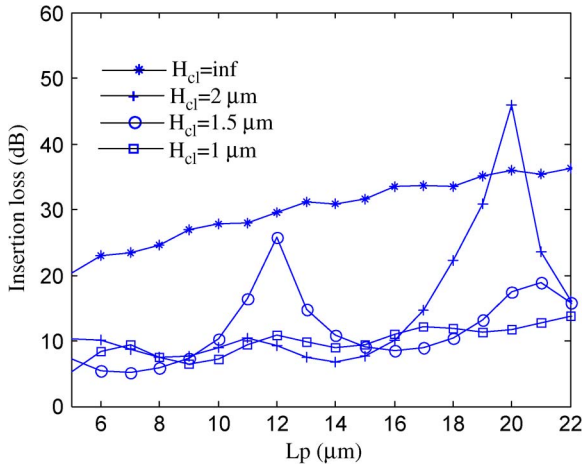

Fig. 6. Insertion loss of the TE mode under different length of the central waveguide and thickness of the buried silicon dioxide layer; calculation is based on a 2-D model with the wide-angle beam propagation method.

propagating light and radiated light reflected back from the substrate. Due to this coupling, the insertion loss reaches the maximum value at some specific lengths of the central waveguide. For example, when the thickness of the buried SiO_2 layer is $H_{cl} = 1.5\ \mu$m, the maximal insertion loss happens at $L_p = 12\ \mu$m for the TE mode, and when the thickness of the buried SiO_2 layer is $H_{cl} = 2\ \mu$m, it happens at $L_p = 20\ \mu$m. From this approximate design, the waveguide polarizer with a central length of $\sim 12\ \mu$m is recommended for an SOI wafer with a 1.5-μm-thick buried SiO_2 layer.

To numerically verify the performance of the waveguide polarizer designed by the approximate 2-D model, a full-vectorial 3-D parallel finite-difference-time-domain simulation is carried out, in which the grid size is chosen to be $\Delta x = \Delta y = \Delta z = 20$ nm (which is less than $\lambda/20$; λ is the wavelength in silicon) with a time step of 3.85×10^{-17} s. The cross section of simulation region is 3 μm in the *x*-direction and 3 μm in the *y*-direction, which includes the silicon substrate so that the influence of the substrate on the device performance can be included. As a single computer cannot handle this simulation with a serial coding of FDTD efficiently, a parallel processing using a message-passing interface is employed in our simulation involving a computer cluster. The calculation region is divided into N subregions along the *z*-direction, and each process is used for each subregion. After the field update in the FDTD, exchange of boundary data is carried out between neighboring subregions.

With the electromagnetic field calculated by the parallel 3-D FDTD simulation, the insertion loss is calculated based on an overlap integral using the Gram–Schmidt orthogonalization technique [18]. For the TE mode under different lengths of the central section, the corresponding insertion losses are presented in Fig. 7 for three cases with different thickness of the buried SiO_2 layer, i.e., semi-infinite, 1.0 μm, and 1.5 μm. The numerical results obtained by the parallel 3-D FDTD basically agree with the above approximate design, and according to this, it is shown that in the case where the thickness of buried SiO_2 is 1.5 μm, the insertion loss for the TE mode reaches the maximal value $\sim$26 dB when the length of the central waveguide is 10 μm. The insertion loss for the TM mode $(H_{cl} = 1.5\ \mu\text{m})$ under a different length of the central waveguide is also presented in Fig. 7, which shows that for the TM mode, the insertion loss is negligible, regardless of the length of the device (which is $\sim 7 \times 10^{-4}$ dB when the central length is 10 μm). For this FDTD simulation, the numerical error is estimated using the 2-D waveguide polarizer model presented in Fig. 5(a) (to characterize the numerical error directly on the 3-D waveguide polarizer requires a dramatic incensement of computational time and resources). We compared the simulation results of waveguide polarizer designed for different a grid size, ranging from 30 nm down to 10 nm. It is found that for the TE mode, the numerical error is found to be $\sim$1 dB (26.83 dB–27.88 dB), and for the TM mode, the numerical error is $\sim$0.2 dB ($-$0.14 dB–0.06 dB).

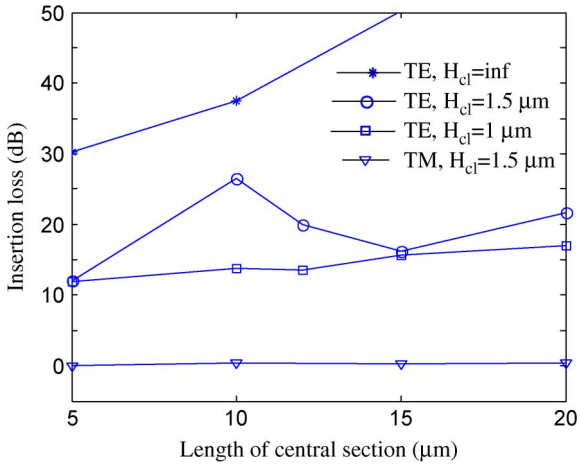

Fig. 7. Insertion loss of the TM-pass polarizer under different lengths of central section calculated by full-vectorial parallel FDTD simulation.

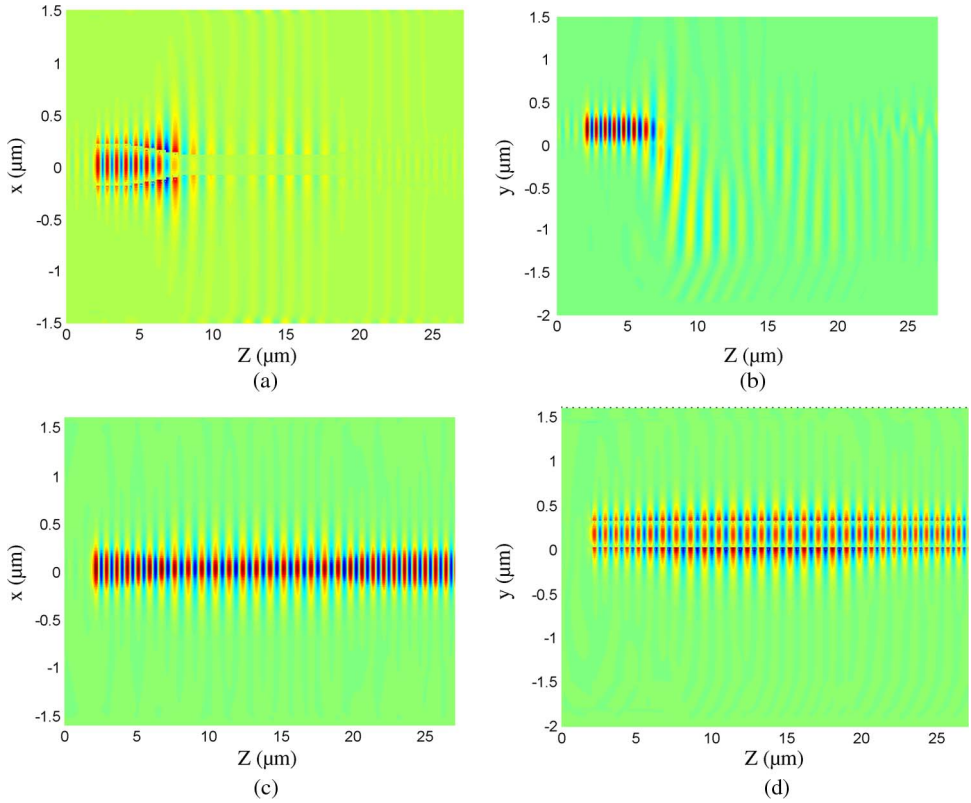

Fig. 8. Simulation of light propagation in the waveguide polarizer ($L_p = 10$ um, $H_{cl} = 1.5$ um) by the 3-D FDTD. (a) TE mode in the *x*–*z* plane. (b) TE mode in the *y*–*z* plane. (c) TM mode in the *x*–*z* plane. (d) TM mode in the *y*–*z* plane.

Simulation results of the light propagation based on the parallel 3-D-FDTD for the TE and TM mode with a central length of $L_p = 10$ μm are presented in Fig. 8. Fig. 8(a) gives the light propagation within the *x*–*z* plane for the TE mode at the middle of the waveguide core in the *y*-direction, which shows that the light is attenuated when propagating along the device. Fig. 8(b) shows the light propagation within *y*–*z* plane for the TE mode at the middle of the waveguide core in the *x*-direction,

and it can be seen that the light radiates away from the waveguide core and is reflected back at the interface between the buried cladding layer and substrate and is coupled with the light propagating in the core. Fig. 8(c) and (d) give the simulation results of light propagation for the TM mode, and it can be seen that the light passes through the structure with ignorable loss.

4. Conclusion

An ultracompact nanophotonic waveguide polarizer based on a simple tapered structure has been proposed, designed, and demonstrated numerically. With a full-vectorial eigenmode solution, a silicon nanophotonic waveguide with a height of 300 nm can only support the TM mode when the width is between 250 nm and 180 nm. The length of the central waveguide is optimized for a high extinction ratio and ultracompact size while taking account of the finite thickness of buried dioxide layer using an approximate 2-D model. Parallel full-vectorial 3-D FDTD has been used to verify the performance of the designed device. The numerical result has shown an extinction ratio $\sim$26 dB for the nanophotonic waveguide polarizer with a central length of 10 μm, while the insertion loss for the TM mode is ignorable.

References

[1] W. Bogaerts, R. Baets, P. Dumon, V. Wiaux, S. Beckx, D. Taillaert, B. Luyssaert, J. Van Campenhout, P. Bienstman, and D. Van Thourhout, "Nanophotonic waveguides in silicon-on-insulator fabricated with CMOS technology," *J. Lightw. Technol.*, vol. 23, no. 1, pp. 401–412, Jan. 2005.

[2] A. Sakai, T. Fukazawa, and T. Baba, "Low loss ultra-small branches in a silicon photonic wire waveguide," *IEICE Trans. Electron.*, vol. E85-C, no. 4, pp. 1033–1038, 2002.

[3] F. Xia, L. Sekaric, M. O'Boyle, and Y. Vlasov, "Coupled resonator optical waveguides based on silicon-on-insulator photonic wires," *Appl. Phys. Lett.*, vol. 89, no. 4, p. 041122, 2006.

[4] K. Sasaki, F. Ohno, A. Motegi, and T. Baba, "Arrayed waveguide grating of 70 $\times$ 60 μm^2 size based on Si photonic wire waveguides," *Electron. Lett.*, vol. 41, no. 14, pp. 801–802, Jul. 2005.

[5] D. Dai, L. Liu, L. Wosinski, and S. He, "Design and fabrication of ultra-small overlapped AWG demultiplexer based on α-Si nanowire waveguides," *Electron. Lett.*, vol. 42, no. 7, pp. 400–402, Mar. 2006.

[6] J. Brouckaert, W. Bogaerts, P. Dumon, D. Van Thourhout, and R. Baets, "Planar concave grating demultiplexer fabricated on a nanophotonic silicon-on-insulator platform," *J. Lightw. Technol.*, vol. 25, no. 5, pp. 1269–1275, May 2007.

[7] A. Densmore, D.-X. Xu, P. Waldron, S. Janz, P. Cheben, J. Lapointe, A. Delage, B. Lamontagne, J. H. Schmid, and E. Post, "A silicon-on-insulator photonic wire based evanescent field sensor," *IEEE Photon. Technol. Lett.*, vol. 18, no. 23, pp. 2520–2522, Dec. 2006.

[8] A. Morand, C. S. Perez, P. Benech, S. Tedjini, and D. Bosc, "Integrated optical waveguide polarizer on glass with a birefringent polymer overlay," *IEEE Photon. Technol. Lett.*, vol. 10, no. 11, pp. 1599–1601, Nov. 1998.

[9] Y. Tong and W. Yizun, "Theoretical study of metal-clad optical waveguide polarizer," *IEEE J. Quantum Electron.*, vol. 25, no. 6, pp. 1209–1213, Jun. 1989.

[10] Y. Kokubun and S. Asakawa, "ARROW-type polarizer utilizing form birefringence in multiplayer first cladding," *IEEE Photon. Technol. Lett.*, vol. 5, no. 12, pp. 1418–1420, Dec. 1993.

[11] M. Bloemer and J. W. Haus, "Broadband waveguide polarizers based on the anisotropic optical constants of nanocomposite films," *J. Lightw. Technol.*, vol. 14, no. 6, pp. 1534–1540, Jun. 1996.

[12] C. Chen and L. Wang, "Design of finite-length metal-clad optical waveguide polarizer," *IEEE J. Quantum Electron.*, vol. 34, no. 7, pp. 1089–1097, Jul. 1998.

[13] C. Chen, L. Pang, C. Tsai, U. Levy, and Y. Fainman, "Compact and integrated TM-pass waveguide polarizer," *Opt. Exp.*, vol. 13, no. 14, pp. 5347–5352, Jul. 2005.

[14] G. R. Hadley, "Multistep method for wide-angle beam propagation," *Opt. Lett.*, vol. 17, no. 24, pp. 1743–1745, Dec. 1992.

[15] A. Taflove and S. C. Hagness, *Computational Electrodynamics: The Finite-Difference Time-Domain Method*. Norwood, MA: Artech House, 2000.

[16] J. Yamauchi, G. Takahashi, and H. Nakano, "Full-vectorial beam propagation method based on the McKee-Mitchell scheme with improved finite-difference formulas," *J. Lightw. Technol.*, vol. 16, no. 12, pp. 2458–2464, Dec. 1998.

[17] Y. He and F. G. Shi, "Improved full-vectorial beam propagation method with high accuracy for arbitrary optical waveguides," *IEEE Photon. Technol. Lett.*, vol. 15, no. 10, pp. 1381–1383, Oct. 2003.

[18] J. Yamauchi, T. Mugita, and H. Nakano, "Implicit Yee-mesh-based finite-difference full vector beam-propagation method," *J. Lightw. Technol.*, vol. 23, no. 5, pp. 1947–1955, May 2005.